PAPER

Continuity of phonon dispersion curves in layered ionic materials

IOP Publishing Journal of Physics: Condensed Matter
J. Phys.: Condens. Matter **32** (2020) 055402 (9pp) https://doi.org/10.1088/1361-648X/ab4cc1

Continuity of phonon dispersion curves in layered ionic materials

Yan Li, W C Kerr and N A W Holzwarth

Physics Department, Wake Forest University, Winston-Salem, NC, United States of America

E-mail: natalie@wfu.edu

Received 1 August 2019, revised 26 September 2019
Accepted for publication 10 October 2019
Published 1 November 2019

Abstract

The coupling of lattice vibrations with macroscopic electric fields in ionic crystals is examined from first principles based on density functional theory and density functional perturbation theory. Our analyses show that the coupled optical phonon–photon modes are well represented by using the pure phonon modes evaluated at $\mathbf{q} = 0$ as a basis. In addition, we find that apparent 'discontinuities' and mode 'disappearances' in the phonon dispersion curves of ionic materials for $\mathbf{q} \to 0$ in hexagonal and other anisotropic materials are caused by the directional dependence of the Born effective charge tensor which is responsible for this coupling. The full dispersion curves, including the phonon–photon transverse modes are shown to be continuous functions of wavevector. Our work in this report provides a promising tool for first principles evaluation of phonon polaritons that may be accessible to experiment. Explicit examples are explored for cubic and hexagonal BN; the calculated results are in good agreement with previous computational values and available experimental measurements.

Keywords: phonon-polariton, first principles calculations, ionic crystals

(Some figures may appear in colour only in the online journal)

1. Introduction

Intuitively, physical quantities are expected to be continuous functions of their variables, so it is a surprise to find discontinuities in phonon dispersion curves. Figure 1 shows a typical representation of phonon dispersion, where the normal mode frequencies $\omega^{\nu}(\mathbf{q})$ are plotted as a function of phonon wavevector $\mathbf{q}$ along special directions of the Brillouin zone for boron nitride in the zincblende structure[1]. For this cubic structure, the phonon dispersion curves $\omega^{\nu}(\mathbf{q})$ appear to be continuous functions of $\mathbf{q}$. By contrast, in examining phonon dispersion curves for ionic materials having hexagonal or other layered structures [1], we often find apparent discontinuities or mode disappearances near the $\mathbf{\Gamma}$ point of the Brillouin zone. For example, figure 2 shows the phonon dispersion curves for boron nitride in the hexagonal structure. For this hexagonal structure, two of the optic phonon dispersion curves with wavevector $\mathbf{q}$ pointing in a direction within a layer plane ($\mathbf{M} \to \mathbf{\Gamma}$) end abruptly at the $\mathbf{\Gamma}$ point and seem to have no presence in the phonon band diagram for the wavevector $\mathbf{q}$ pointing in the perpendicular direction ($\mathbf{\Gamma} \to \mathbf{A}$). In reality, the phonon band diagram represents the same number of vibrational modes (in this case 12) throughout the Brillouin zone.

The physical reasons for these discontinuities were explained in 1951 by Huang [2] and are detailed in several textbooks [3–6]. The explanation is based on the analysis of the coupling of some of the vibrational modes to long wavelength electromagnetic waves within the material including the effects of Maxwell's equations on the system. In this report, we show how the dispersion curves of the coupled phonon–photon modes can be calculated from first principles and can be included in a modified phonon band diagram in the $|\mathbf{q}| \to 0$ range. The photon-phonon normal modes of cubic and hexagonal BN are examined as examples.

The remainder of this paper is organized as follows. Section 2 details the general formalism. Section 3 presents the results for BN, including a description of the first principles methods (section 3.1) and results for the phonon–photon dispersions in the vicinity of $\mathbf{q} \to 0$ range for cubic and

[1] Following usual practices, for plotting and tabulation purposes, instead of representing frequencies in radians per second, we use throughout the manuscript $\omega^{\nu}(\mathbf{q})/(2\pi c)$ in units of (cm^{-1}). Here c denotes the speed of light in vacuum.

hexagonal BN (section 3.2). Section 4 contains the summary and conclusions.

2. Formalism

The first principles formalism for evaluating vibrational modes of periodic solids within the framework of the Born–Oppenheimer approximation [3] and density functional theory [8, 9], has been developed using density functional perturbation theory (DFPT) by a number of authors [10–14]. This formalism has been implemented in several electronic structure code packages such as ABINIT [15] and Quantum ESPRESSO [16]. In the following, we approximately follow the notation of [13] and [14], using Gaussian units.

The starting point of the analysis is a self-consistent density functional calculation to find the optimized total energy of the crystalline material, finding the optimized lattice vectors **a**, **b**, and **c**, the optimized coordinates $\boldsymbol{\tau}_s$ of the N atoms labeled s within the unit cell, and the corresponding static lattice energy per unit cell U_{SL}. Here $\boldsymbol{\tau}_s$ represents the equilibrium position within a unit cell and any given cell within the material can be represented relative to the origin by a translation vector $\mathbf{R}_l = l_1\mathbf{a} + l_2\mathbf{b} + l_3\mathbf{c}$ where l_i denote integer values. Consider that an optimized atomic position in unit cell at position $\mathbf{R}_l$ is displaced by a small vector $\mathbf{u}_s(l)$.

$$\mathbf{R}_l + \boldsymbol{\tau}_s \rightarrow \mathbf{R}_l + \boldsymbol{\tau}_s + \mathbf{u}_s(l). \tag{1}$$

It is convenient to perform the analysis in phonon wavevector space. For a given phonon wavevector $\mathbf{q}$ within the Brillouin zone,

$$\mathbf{u}_s(l) = \mathbf{u}_s(\mathbf{q})\mathrm{e}^{\mathrm{i}\mathbf{q}\cdot\mathbf{R}_l}, \tag{2}$$

where $\mathbf{u}_s(\mathbf{q})$ represents the complex amplitude of the atomic displacement associated with atom s and wavevector $\mathbf{q}$. Then, within the harmonic approximation, and using DFPT, it is possible to evaluate the analytic part of the second derivative matrix

$$\tilde{C}_{s\alpha,t\beta}(\mathbf{q}) = \frac{\partial^2 U_{SL}}{\partial u^*_{s\alpha}(\mathbf{q})\partial u_{t\beta}(\mathbf{q})}. \tag{3}$$

Here, α and β denote the Cartesian coordinate directions x, y, or z. For most of the Brillouin zone where $|\mathbf{q}| > 0$, and within the Born–Oppenheimer approximation [3], the ion motion can be determined from the classical equations of motion in terms of the harmonic restoring force represented by the second derivative matrix (equation (3)) according to the equation

$$M_s\frac{\partial^2 u_{s\alpha}(\mathbf{q})}{\partial t^2} = -\sum_{t\beta}\tilde{C}_{s\alpha,t\beta}(\mathbf{q})u_{t\beta}(\mathbf{q}). \tag{4}$$

Here, M_s denotes the mass of atom s. In this analysis, we have assumed that the displacement is a continuous function of time t according to $\mathbf{u}_s(\mathbf{q}) \rightarrow \mathbf{u}_s(\mathbf{q}, t) \rightarrow \mathbf{u}_s(\mathbf{q})\mathrm{e}^{-\mathrm{i}\omega t}$, where the last expression includes the further assumption of a harmonic time dependence. Typically these equations are solved in terms of normal modes of vibration with eigenfrequencies ω^ν and eigendisplacements $u^\nu_{s\alpha}$:

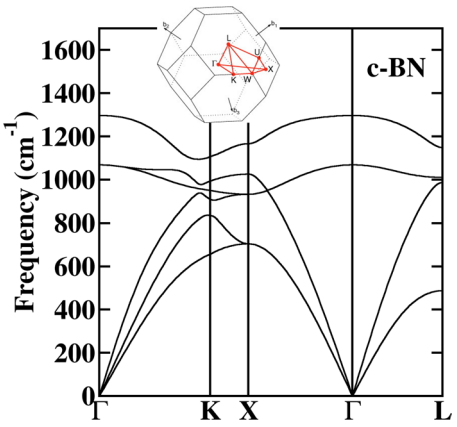

Figure 1. Phonon dispersion curves $(\omega^\nu(\mathbf{q}))$ for cubic BN. The inset Brillouin zone diagram was reprinted from Setyawan *et al* [7], copyright (2010), with permission from Elsevier.

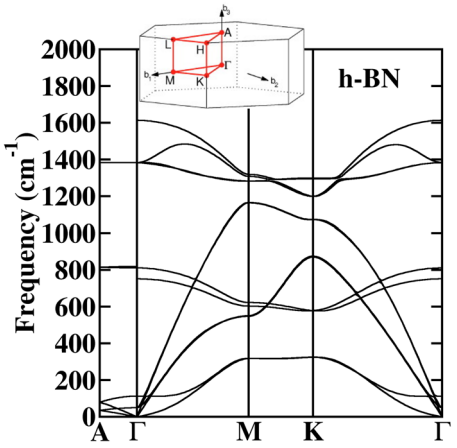

Figure 2. Phonon dispersion curves $(\omega^\nu(\mathbf{q}))$ for hexagonal BN. The inset Brillouin zone diagram was reprinted from Setyawan *et al* [7], copyright (2010), with permission from Elsevier.

$$(\omega^\nu(\mathbf{q}))^2 M_s u^\nu_{s\alpha}(\mathbf{q}) = \sum_{t\beta}\tilde{C}_{s\alpha,t\beta}(\mathbf{q})u^\nu_{t\beta}(\mathbf{q}), \tag{5}$$

where ν labels each of the $3N$ normal mode solutions corresponding to a unit cell with N atoms. It is convenient to normalize the eigendisplacements according to

$$\sum_{s\alpha}|u^\nu_{s\alpha}(\mathbf{q})|^2 = 1. \tag{6}$$

Note that the eigendisplacements satisfy an orthogonality condition

$$\sum_{s\alpha}M_s\left(u^{\nu'}_{s\alpha}(\mathbf{q})\right)^* u^\nu_{s\alpha}(\mathbf{q}) = M^\nu\delta_{\nu'\nu}, \tag{7}$$

where M^ν denotes a mode effective mass.

However, in the long wavelength limit as $\mathbf{q} \rightarrow 0$, the ionic motion couples to the macroscopic electric field. The coupling depends on the Born effective charge tensor for each atom [17] which can be calculated by evaluating the response of the system to an electric field using DFPT. A convenient expression for the Born effective charge tensor is

$$eZ^{*s}_{\alpha\beta} = -\left.\frac{\partial^2 U_{SL}}{\partial u_{s\alpha}(\mathbf{q}=0)\partial E_\beta}\right|_{u_{s\alpha}=0,E_\beta=0}. \tag{8}$$

Here e denotes the elementary charge and E_β denotes an electric field in the β direction and the derivative is evaluated in the limit of zero field value. We note the asterisk in the notation (equation (8)) does not imply complex conjugation [12]. It can be shown [12, 18] that the Born effective charge tensor satisfies the relation for each combination of $\alpha\beta$

$$\sum_s Z^{*s}_{\alpha\beta} = 0. \tag{9}$$

On the other hand, the tensor properties of $Z^{*s}_{\alpha\beta}$ depend on the site symmetry of atom s and for some materials it is possible that the Born effective charge tensor is not symmetric such that [19]

$$Z^{*s}_{\alpha\beta} \neq Z^{*s}_{\beta\alpha}. \tag{10}$$

Because of the coupling of the ion motion to the long wavelength electric field, in the $\mathbf{q} \to 0$ range, the ionic displacements are described by the modified equations of motion determined by both the harmonic restoring force represented by the second derivative matrix (equation (3)) and the coupling due to the Born effective charge tensor (equation (8)) to an electric field.

$$M_s \frac{\partial^2 w_{s\alpha}(\mathbf{q})}{\partial t^2} = -\sum_{t\beta} \tilde{C}_{s\alpha,t\beta}(\mathbf{q}) w_{t\beta}(\mathbf{q}) + \sum_\beta eZ^{*s}_{\alpha\beta} E_\beta(\mathbf{q}). \tag{11}$$

Here we introduced the notation $\mathbf{w}_s(\mathbf{q}) \to \mathbf{w}_s(\mathbf{q},t) \to \mathbf{w}_s(\mathbf{q})e^{-i\omega t}$ to represent the atomic displacements coupled to the electric field in order to distinguish them from their uncoupled counter parts $\mathbf{u}_s(\mathbf{q})$. In turn, the related electric displacement field $\mathbf{D}(\mathbf{q})$ is composed of electric field $\mathbf{E}(\mathbf{q})$ screened by the electronic response as characterized by the electronic part of the dielectric permittivity tensor which is often denoted as $\epsilon^\infty_{\alpha\beta}$ and the additional polarization field introduced by the vibrating ions according to:

$$D_\alpha(\mathbf{q}) = \sum_\beta \epsilon^\infty_{\alpha\beta} E_\beta(\mathbf{q}) + \frac{4\pi e}{\Omega} \sum_{t\beta} Z^{*t}_{\alpha\beta} w_{t\beta}(\mathbf{q}). \tag{12}$$

Here Ω denotes the volume of the unit cell.

We assume that our material is insulating and neutral so that the sourceless Maxwell's equations apply. We also assume that there are no magnetic dipolar effects so that the two relations for the electric and displacement fields in the $\mathbf{q} \to 0$ range resulting from Maxwell's equations are given by

$$\nabla \cdot \mathbf{D} = 0, \tag{13}$$

and

$$\nabla \times (\nabla \times \mathbf{E}) + \frac{1}{c^2}\frac{\partial^2 \mathbf{D}}{\partial t^2} = 0. \tag{14}$$

In this $\mathbf{q} \to 0$ range, we approximate the lattice displacements as continuous functions of position responding to the macroscopic electric and magnetic fields within the material, seeking plane-wave-like solutions with

$$\mathbf{w}_s(l) \to \mathbf{w}^0_s(\mathbf{q})e^{i\mathbf{q}\cdot\mathbf{r}-i\omega t} \text{ and } \mathbf{E}(\mathbf{q}) = \mathbf{E}^0(\mathbf{q})e^{i\mathbf{q}\cdot\mathbf{r}-i\omega t}. \tag{15}$$

In order to solve the coupled equations (11), (13) and (14), it is reasonable to assume that the amplitude of the displacements can be expressed as a linear combination of the pure vibrational normal modes with unknown amplitudes U^ν

$$w^0_{s\alpha}(\mathbf{q}) = \sum_\nu U^\nu(\mathbf{q}) u^\nu_{s\alpha}(\mathbf{q}). \tag{16}$$

Since the analysis is performed in the $\mathbf{q} \to 0$ limit the amplitude and eigenvectors can be evaluated at $\mathbf{q} = 0$. Accordingly we will drop the $\mathbf{q}$ argument in most of the following analysis. The coupling effects of the atomic motions and the electric field are controlled by the sum of the Born effective charges multiplied by the normal mode displacements which can be evaluated for each normal mode. It is convenient to define two summations according to

$$\mathcal{R}^\nu_\alpha \equiv \sum_{t\beta} Z^{*t}_{\alpha\beta} u^\nu_{t\beta} \tag{17}$$

and

$$\mathcal{L}^\nu_\beta \equiv \sum_{s\alpha} (u^\nu_{s\alpha})^* Z^{*s}_{\alpha\beta}. \tag{18}$$

For many modes ν, the Born coupling parameters are trivial; $\mathcal{L}^\nu_\beta = \mathcal{R}^\nu_\beta = 0$. Non-trivial values of $\mathcal{L}^\nu_\beta$ and $\mathcal{R}^\nu_\beta$ indicate that for this mode, the displacement eigenvector creates an oscillating electrical polarization which typically interacts with external infrared radiation. For nontrivial modes, the two coupling parameters $\mathcal{L}^\nu_\beta$ and $\mathcal{R}^\nu_\beta$ need not be related. However for crystalline materials having atomic sites with high symmetry such that relationships in equation (10) are equalities, the two coefficients are related according to $\mathcal{R}^\nu_\alpha = (\mathcal{L}^\nu_\alpha)^*$. By using the expansion (equation (16)) to evaluate the equation of motion for the displacements (equation (11)), we find that the amplitudes U^ν are proportional to the electric field according to

$$U^\nu = \frac{e}{\left((\omega^\nu)^2 - \omega^2\right) M^\nu} \sum_\beta \mathcal{L}^\nu_\beta E^0_\beta. \tag{19}$$

These amplitudes can be used in equation (12) to evaluate the frequency-dependent electric displacement field and the corresponding frequency-dependent dielectric tensor according to

$$\epsilon_{\alpha\beta}(\omega) = \epsilon^\infty_{\alpha\beta} + \frac{4\pi e^2}{\Omega} \sum_\nu \frac{\mathcal{R}^\nu_\alpha \mathcal{L}^\nu_\beta}{\left((\omega^\nu)^2 - \omega^2\right) M^\nu}. \tag{20}$$

This expression is equivalent to a similar analysis by Gonze and Lee [12] and some of the ideas are presented in textbooks such as Maradudin *et al* [5]. Equation (20) is valid for frequencies ω small enough such that $\hbar\omega < E_g$, where E_g represents the electronic band gap. This restriction is consistent with the assumption that the electronic dielectric contribution $\epsilon^\infty_{\alpha\beta}$ is constant. The estimation of the static dielectric constant, $\epsilon^0_{\alpha\beta}$, evaluated by setting $\omega \to 0$ is expected to be well justified by the expression

$$\epsilon^0_{\alpha\beta} \equiv \epsilon_{\alpha\beta}(\omega = 0) = \epsilon^\infty_{\alpha\beta} + \frac{4\pi e^2}{\Omega} \sum_\nu \frac{\mathcal{R}^\nu_\alpha \mathcal{L}^\nu_\beta}{(\omega^\nu)^2 M^\nu}. \quad (21)$$

It is interesting to mention that equation (20) is consistent with a Drude-like model of the ionic contributions to the dielectric function, where $(\mathcal{R}^\nu_\alpha \mathcal{L}^\nu_\beta)/(M^\nu/m_e)$ represents an oscillator strength, with m_e denoting the electron mass. Missing from the analysis and from equation (20) are considerations of damping processes that may more fully describe the driven oscillator system. Using the notation γ^ν to represent the damping coefficient for mode ν, equation (20) would be modified with an imaginary contribution with alteration of the denominator

$$\left((\omega^\nu)^2 - \omega^2\right) \rightarrow \left((\omega^\nu)^2 - \omega^2 - i\omega\gamma^\nu\right). \quad (22)$$

However, these damping effects are outside the scope of the present study.

In order to now solve Maxwell's equations (equations (13) and (14)) in the long wavelength limit, we consider two cases in terms of the orientation of the wavevector $\mathbf{q}$ relative to the electric field orientation. For the case of a longitudinal electric field, the electric field is along the wavevector direction as represented by the unit vector $\hat{\mathbf{q}}$; $E^0_L = \mathbf{E}^0 \cdot \hat{\mathbf{q}}$. For the case of a transverse electric field, it is convenient to define the propagation direction $\hat{\mathbf{q}}$ and two perpendicular transverse directions denoted by unit vectors $\hat{\mathbf{T}}_1$ and $\hat{\mathbf{T}}_2$. In this case the electric field $\mathbf{E}^0_T$ is in the plane spanned by $\mathbf{T}_1$ and $\mathbf{T}_2$. For example, the longitudinal and transverse matrix elements of the electronic dielectric tensor can be written

$$\epsilon^\infty_{LL} \equiv \sum_{\alpha\beta} \hat{q}_\alpha \epsilon^\infty_{\alpha\beta} \hat{q}_\beta \quad \text{and} \quad \epsilon^\infty_{T_iT_j} \equiv \sum_{\alpha\beta} \hat{T}_{i\alpha} \epsilon^\infty_{\alpha\beta} \hat{T}_{j\beta}, \quad (23)$$

where $i,j = 1,2$. Similarly, we can define longitudinal and transverse components of the Born coupling parameters such as

$$\mathcal{R}^\nu_L \equiv \sum_\alpha \mathcal{R}^\nu_\alpha \hat{q}_\alpha \quad \text{and} \quad \mathcal{L}^\nu_L \equiv \sum_\beta \mathcal{L}^\nu_\beta \hat{q}_\beta \quad (24)$$

for the longitudinal Born coupling parameters, and similar expressions can be written for the transverse coupling parameters.

In the following analysis, we assume that the dielectric tensor (equation (20)) is block diagonal in the directions $\hat{\mathbf{q}}$, $\hat{\mathbf{T}}_1$, and $\hat{\mathbf{T}}_2$, Mixed longitudinal and transverse solutions will not be considered in this analysis.

For the longitudinal solutions, the $\mathbf{E}$ and $\mathbf{D}$ fields both are along the direction $\hat{\mathbf{q}}$. However, Maxwell's equations (equations (13) and (14)) require that the longitudinal component of the frequency-dependent dielectric tensor (equation (20)) vanishes:

$$\epsilon_{LL} = \epsilon^\infty_{LL} + \frac{4\pi e^2}{\Omega} \sum_\nu \frac{\mathcal{R}^\nu_L \mathcal{L}^\nu_L}{\left((\omega^\nu)^2 - \omega^2\right) M^\nu} = 0. \quad (25)$$

Here, the summation is taken only over nontrivial modes ν. For any given longitudinal direction $\hat{\mathbf{q}}$, the number n_L of nontrivial values of longitudinal Born coupling parameters $\mathcal{R}^\nu_L$ and $\mathcal{L}^\nu_L$ is less than the total number of normal modes ($3N$). The general solution of equation (25) requires the solution of a n^{th}_L order polynomial in the variable ω^2. In the special case that $n_L = 1$ and the nontrivial mode is written with index ν, the solution to equation (25) takes the form

$$\omega^2 \equiv \omega^2_L = (\omega^\nu)^2 + \frac{1}{\epsilon^\infty_{LL}} \frac{4\pi e^2}{\Omega M^\nu} \mathcal{R}^\nu_L \mathcal{L}^\nu_L. \quad (26)$$

This longitudinal 'LO' mode does not depend on $\mathbf{q}$.

An alternative approach was developed by Giannozzi and others [10, 12, 13] and included in the ABINIT and QUANTUM ESPRESSO codes, for example, combining the longitudinal component of equation (12) with the longitudinal component of equation (11) to directly solve for the $\mathbf{q} \rightarrow 0$ longitudinal modes according to the equation

$$\omega^2 M_s w^0_{s\alpha}(\mathbf{q}) = \sum_{t\beta} \tilde{C}^{\text{tot}}_{s\alpha,t\beta}(\mathbf{q}) w^0_{t\beta}(\mathbf{q}). \quad (27)$$

Here

$$\tilde{C}^{\text{tot}}_{s\alpha,t\beta}(\mathbf{q}) = \tilde{C}_{s\alpha,t\beta}(\mathbf{q}) + \frac{4\pi e^2}{\Omega \epsilon^\infty_{LL}} Z^{*s}_{L\alpha} Z^{*t}_{\beta L}. \quad (28)$$

The second term of equation (28) is usually referenced as the non-analytic contribution to the second derivative matrix. The direct solution of equation (27) gives the corrected eigenmodes of the longitudinal atomic displacements in the $\mathbf{q} \rightarrow 0$ range. Note that for this longitudinal case, even though the long wavelength electrical field is polarized in the longitudinal direction, some of the atomic displacements may have components in other directions. It has been noted by Gonze and Lee [12] that the eigenvectors of equation (27) are not necessarily the same as the eigenvectors of equation (5). In fact, if we use the pure phonon mode basis to represent the atomic displacements in equation (27) as in equation (16), we see that the non-analytic term can cause mixing of the pure phonon modes. It is possible to determine the n_L eigenvalues ω^2_L of equation (27) by diagonalizing a $n_L \times n_L$ matrix $\mathcal{G}^L_{\nu\nu'}$ in the pure phonon mode basis.

$$\sum_{\nu'} \mathcal{G}^L_{\nu\nu'} U^{\nu'} = \omega^2_L U^\nu. \quad (29)$$

The matrix elements are given by

$$\mathcal{G}^L_{\nu\nu'} = (\omega^\nu)^2 \delta_{\nu\nu'} + \frac{1}{\epsilon^\infty_{LL}} \frac{4\pi e^2}{\Omega M^\nu} \mathcal{L}^\nu_L \mathcal{R}^{\nu'}_L. \quad (30)$$

This is equivalent to solving the polynomial equation implied by equation (25) or to directly solving equation (27). However, the advantage of solving the eigenvalue problem of equation (29) is that for each eigenvalue ω^2_L, one can also determine the corresponding eigenvector in terms of the amplitudes U^ν of the n_L coupled pure phonon modes.

For the transverse solutions, Maxwell's equation (13) is always satisfied since the wavevector is perpendicular the electric field direction, while Maxwell's equation (14) describes another $\mathbf{q}$-dependent coupling relationship between

the fields and ion motions. The solutions $\omega^2 = \omega_T^2$ must satisfy Maxwell's equations for the transverse case according to the following relationships:

$$\sum_{T_j}\left(q^2c^2\delta_{T_iT_j} - \omega_T^2\left(\epsilon^{\infty}_{T_iT_j} + \frac{4\pi e^2}{\Omega}\sum_{\nu}\frac{\mathcal{R}^{\nu}_{T_i}\mathcal{L}^{\nu}_{T_j}}{\left(\left(\omega^{\nu}\right)^2 - \omega_T^2\right)M^{\nu}}\right)\right)E^0_{T_j} = 0. \tag{31}$$

For any given choice of transverse directions $\hat{\mathbf{T}}_i$ and $\hat{\mathbf{T}}_j$, the number n_T of nontrivial values of the transverse Born coupling parameters $\mathcal{R}^{\nu}_{T_i}$ and $\mathcal{L}^{\nu}_{T_j}$ is less than the total number of normal modes ($3N$). The general solutions of equation (31) requires the solution of a $2n_T^{\text{th}}$ order polynomial in the variable ω^2. In the special case that $n_T = 1$, the transverse electronic dielectric tensor $\epsilon^{\infty}_{T_iT_j}$ is diagonal, and the nontrivial mode is written with index ν, the solution to equation (31) for a given value of the wavevector q, takes the form

$$\omega^2_{T_i\pm}(\mathbf{q}) = \frac{q^2c^2 + \left(\omega^{\nu}\right)^2\epsilon^{\infty}_{T_iT_i} + \mathcal{A}^{\nu}}{2\epsilon^{\infty}_{T_iT_i}}\left(1 \pm \mathcal{S}^{\nu}(\mathbf{q})\right). \tag{32}$$

Here,

$$\mathcal{S}^{\nu}(\mathbf{q}) \equiv \sqrt{1 - \frac{4q^2c^2\left(\omega^{\nu}\right)^2\epsilon^{\infty}_{T_iT_i}}{\left(q^2c^2 + \left(\omega^{\nu}\right)^2\epsilon^{\infty}_{T_iT_i} + \mathcal{A}^{\nu}\right)^2}}, \tag{33}$$

and

$$\mathcal{A}^{\nu} \equiv \frac{4\pi e^2}{\Omega M^{\nu}}\mathcal{R}^{\nu}_{T_i}\mathcal{L}^{\nu}_{T_i}. \tag{34}$$

In the neighborhood of $\mathbf{q} = 0$, the '+' branch of the transverse modes takes the value

$$\omega^2_{T_i+}(\mathbf{q} \approx 0) = \left(\omega^{\nu}\right)^2 + \frac{1}{\epsilon^{\infty}_{T_iT_i}}\frac{4\pi e^2}{\Omega M^{\nu}}\mathcal{R}^{\nu}_{T_i}\mathcal{L}^{\nu}_{T_i} + Sq^2c^2. \tag{35}$$

The value of $\omega^2_{T_i+}(\mathbf{q} = 0)$ is numerically the same as the longitudinal solution in equation (26) when the electric field directions are geometrically the same. For $q > 0$, the dispersion is that of a photon mode with quadratic coefficient $S = 1/\epsilon^{\infty}_{T_iT_i} - 1/\epsilon^{0}_{T_iT_i}$. The '−' branch of the transverse modes in the $\mathbf{q} \to 0$ range have linear dispersion with the form $\omega_{T_i-}(\mathbf{q}) = qc/\sqrt{\epsilon^0_{T_iT_i}}$ for $\mathbf{q} \approx 0$. For larger values of wavevector, $\mathbf{q} \gg \omega^{\nu}c/\sqrt{\epsilon^{\infty}_{T_iT_i}}$, the frequency of the transverse modes is asymptotic to $\omega_{T_i-}(\mathbf{q}) = \omega^{\nu}$, the normal mode frequency without electric field effects and identifies as a 'TO' mode. In summary, the solution for $\omega_{T_i-}(\mathbf{q})$ is photon-like at very small values of q and becomes phonon-like, at larger values of q. The expressions discussed in this section will be illustrated for the example of BN in section 3.2. More general analysis for choices of the transverse directions $\hat{T}_i$ have been worked out for the case of α-GaN by Irmer *et al* [20] which isostructural to hexagonal BN.

It is also possible to write the general equations for the transverse modes for the case $n_T > 1$ in the pure phonon basis similarly to equation (29). The general expression can be written in terms of a generalized eigenvalue problem of the form

$$\sum_{\nu'}\mathcal{G}^T_{\nu\nu'}U^{\nu'} = \omega_T^2U^{\nu}, \tag{36}$$

where the $n_T \times n_T$ matrix $\mathcal{G}^T_{\nu\nu'}$ is given by

$$\mathcal{G}^T_{\nu\nu'} \equiv \left(\omega^{\nu}\right)^2\delta_{\nu\nu'} + \frac{4\pi e^2}{\Omega M^{\nu}}\sum_{T_iT_j}\left(\boldsymbol{\epsilon}^{\infty} - \frac{q^2c^2}{\omega_T^2}\mathbf{I}\right)^{-1}_{T_iT_j}\mathcal{L}^{\nu}_{T_i}\mathcal{R}^{\nu'}_{T_j}. \tag{37}$$

This is not a usual eigenvalue problem since the eigenvalue ω_T^2 appears in the expression of the matrix $\mathcal{G}^T_{\nu\nu'}$; however iterative methods can be used to solve equation (36). Because of this, there are generally two solutions for each value of $\mathbf{q}$ corresponding to the $\omega_{T\pm}(\mathbf{q})$ branches. The limiting values of the results for $q = 0$ and $q \gg \omega^{\nu}c/\sqrt{\epsilon^{\infty}_{T_iT_i}}$ derived for the simple case can be seen from the form of equation (37).

Note that in all of these expressions, the value of the phonon–photon coupling is controlled by Born coupling parameters defined in equations (17) and (18) $\mathcal{R}^{\nu}_{\alpha}$ and $\mathcal{L}^{\nu}_{\alpha}$, where α is the direction of the atomic displacements for the pure phonon mode ν. Whether the full solution to the coupled phonon–photon equations is longitudinal or transverse depends on the direction of the wavevector $\mathbf{q}$ relative to the direction α. Because of the form of the non-trivial Born coupling parameters $\mathcal{L}^{\nu}_{\beta}$ and $\mathcal{R}^{\nu}_{\beta}$, the modes ν are often labeled as 'optical' modes 'LO' or 'TO' corresponding to longitudinal or transverse, respectively. The ω_{LO} frequencies are shifted relative to the frequencies ω^{ν} of the pure phonon vibrations according to equations (29) and (30) due to their coupling to the long wavelength electric fields. However the ω_{TO} frequencies correspond to $\omega_{T-}(q \gg \omega^{\nu}c/\sqrt{\epsilon^{\infty}_{T_iT_i}}) = \omega^{\nu}$, that is having the same magnitude as the uncoupled transverse $\mathbf{\Gamma}$ point phonon vibrations. While the ABINIT and QUANTUM ESPRESSO codes do not explicitly consider the coupled transverse phonon–photon modes, all of the necessary parameters are calculated in order to evaluate equations (30) and (37).

3. Example results for cubic and hexagonal BN

While the equations presented in section 2 apply generally to all insulating ionic crystals, it is useful to illustrate the results for the simple and well-studied example of boron nitride so that we can compare with a large literature of experimental [21–28] and computational [29–38] reports.

3.1. Calculational methods

The structural optimizations were based on density functional theory (DFT) [8, 9] and the phonon frequencies and eigenvectors of normal vibrational modes were obtained by diagonalizing the dynamical matrix using density functional perturbation theory (DFPT) [10–14]. The computations used the projector augmented wave (PAW) [39] formalism. The PAW basis and projector functions were generated by the ATOMPAW [40] code. The local density approximation (LDA) [41] functional was chosen to treat the exchange-correlation effects. The calculations were carried out by using

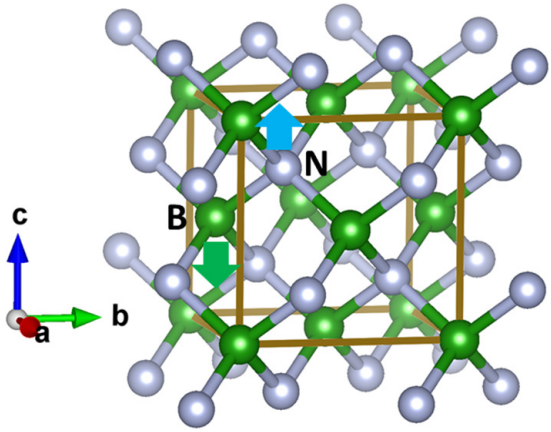

Figure 3. Ball and stick drawing of conventional unit cell of cubic BN (space group $F\bar{4}3m$ [44]) indicating one B and one N site within a primitive cell. The arrows indicate the vibrational directions of the atoms for one of the three degenerate optical modes at $\mathbf{q} = 0$ ($\mathbf{\Gamma}$ point).

Table 1. Comparison of experimental and calculated optical properties of cubic (zincblende) BN, including the electronic (ϵ^{∞}) and static (ϵ^{0}) dielectric constants, Born effective charges ($Z^{*B} = -Z^{*N}$), and frequencies of TO (ω_{TO}) and LO vibrational modes (ω_{LO}) (in units of cm^{-1}).

ϵ^{∞}	ϵ^{0}	Z^{*B}	ω_{TO}	ω_{LO}	Reference
4.55	6.70	1.87	1069	1297	Calc. (Present)
4.5	7.1		1065	1340	Exp. ([22])
4.46	6.80		1056	1305	Exp. ([25])
4.54		1.93	1040	1285	Calc. ([29])
4.54	6.74	1.89	1062	1295	Calc. ([31])
4.52	6.93		1027	1269	Calc. ([34])

the ABINIT package [15] and checked with the Quantum ESPRESSO [16] package. Visualizations were constructed using the XCrySDEN [42] and VESTA [43] software packages.

The results were obtained using very tight convergence tolerances and dense sampling parameters beyond what was actually necessary for convergence. The plane wave expansion of the electronic wavefunctions included wavevectors with $|\mathbf{k} + \mathbf{G}|^2 \leqslant (2m_e/\hbar^2)E_{\mathrm{cut}}$ with $E_{\mathrm{cut}} = 80$ Ry. The electronic structure was sampled on a uniform grid of $16 \times 16 \times 16$ and $12 \times 12 \times 8$ $\mathbf{k}$-points within the Brillouin zone for the cubic and hexagonal structures respectively.

The optimized lattice constant for the cubic cell of BN (space group $F\bar{4}3m$; #216 in the International table of crystallography [44]), was found to be 3.58 Å which compares well with the experimental value [45] of 3.6159 Å measured at room temperature. The optimized lattice constants for the hexagonal cell of BN (space group $P6_3/mmc$; #194 in the International table of crystallography [44]) were found to be $a = 2.49$ Å and $c = 6.49$ Å which compare well with the experimental values [46] of $a = 2.50\,399$ Å and $c = 6.6612$ Å measured at room temperature.

The phonon analysis was performed using density functional perturbation theory, sampling the phonon dispersion on a uniform grid of $4 \times 4 \times 4$ and $6 \times 6 \times 2$ $\mathbf{q}$-points for

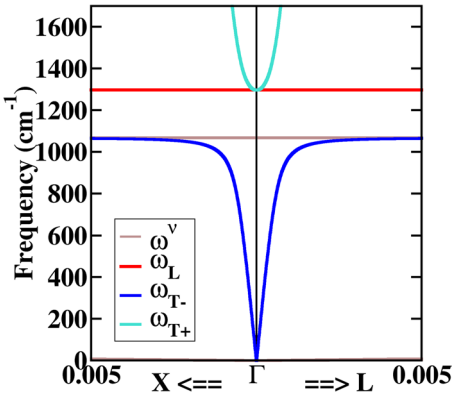

Figure 4. Phonon and phonon–photon dispersion curves in the vicinity of the $\mathbf{\Gamma}$ point of the Brillouin zone for cubic BN. The plot includes $\mathbf{q}$ points in the direction $\mathbf{\Gamma} \rightarrow \mathbf{X}$ and in the direction $\mathbf{\Gamma} \rightarrow \mathbf{L}$ with the 0.005 tick marks indicating the value of $\mathbf{q}$ in units of the length of the $\mathbf{\Gamma} \rightarrow \mathbf{X}$ distance. The end points of the graph correspond to $|\mathbf{q}| = 1.4 \times 10^5$ cm^{-1}. The curves for ω^{ν} represent the modes calculated by ABINIT from equation (5) corrected for the TO-LO splitting as shown in figure 1. The coupled longitudinal modes are plotted in red while the coupled transverse modes are plotted in turquoise for upper branch and blue for lower branch as indicated.

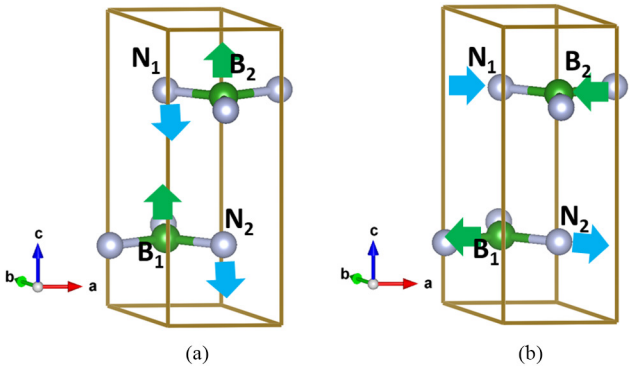

Figure 5. Ball and stick drawing of unit cell of hexagonal BN (space group $P6_3/mmc$ [44]) indicating the four B and N sites. The arrows indicate the vibrational directions of the atoms for $\mathbf{q} = 0$ ($\mathbf{\Gamma}$ point) mode # 7 (a) and for mode # 11 (b).

the cubic and hexagonal structures respectively. These values were used in the ABINIT code to generate the phonon dispersion curves presented in figures 1 and 2; these are consistent with previous calculations in the literature [29, 30, 32, 35].

3.2. Examples of phonon–photon dispersion curves

3.2.1. BN in a cubic structure. Figure 3 shows a diagram of a conventional unit cell of BN in the cubic structure (zincblende with space group $F\bar{4}3m$) with two atoms per primitive unit cell. The corresponding six phonon dispersion curves $\omega^{\nu}(\mathbf{q})$ are presented in figure 1. The upper three curves near the $\mathbf{\Gamma}$ point are optical modes. At the $\mathbf{\Gamma}$ point ($\mathbf{q} = 0$), the single ω_{LO} mode is computed to have frequency $1298\,\mathrm{cm}^{-1}$ while the doubly degenerate ω_{TO} modes are computed to have the frequency $1069\,\mathrm{cm}^{-1}$. These were determined using the ABINIT and QUANTUM ESPRESSO codes which use the 'non-analytic' corrections to the second derivative matrix given in

Table 2. Comparison of experimental and simulated optical properties of hexagonal ($P6_3/mmc$) BN, including the electronic (ϵ^{∞}_{xx}, ϵ^{∞}_{zz}) and static (ϵ^{0}_{xx}, ϵ^{0}_{zz}) dielectric constants and Born effective charges ($Z^{*B}_{xx} = -Z^{*N}_{xx}$, $Z^{*B}_{zz} = -Z^{*N}_{zz}$). Here x refers to the hexagonal plane and z refers to the c axis direction. Also listed are the lower and higher frequency optical mode frequencies in units of cm^{-1}.

ϵ^{∞}_{xx}	ϵ^{∞}_{zz}	ϵ^{0}_{xx}	ϵ^{0}_{zz}	Z^{*B}_{xx}	Z^{*B}_{zz}	$\omega^{\text{low}}_{\text{TO}}$	$\omega^{\text{low}}_{\text{LO}}$	$\omega^{\text{high}}_{\text{TO}}$	$\omega^{\text{high}}_{\text{LO}}$	Reference
4.88	2.85	6.65	3.39	2.70	0.81	752	820	1383	1614	Calc. (Present)
4.95	4.10	7.04	5.09			783	828	1367	1610	Exp. [21]
4.85	2.84	6.61	3.38	2.71	0.82	754	823	1382	1614	Calc. [31]
4.87	2.95	6.71	3.57			746	819	1372	1610	Calc. [34]

equation (27). Because of the high symmetry of this crystal, the dielectric tensors $\epsilon^{\infty}_{\alpha\beta}$ and $\epsilon^{0}_{\alpha\beta}$ are diagonal and isotropic as are the Born effective charge tensors $Z^{*B}_{\alpha\beta} = -Z^{*N}_{\alpha\beta}$. The results computed in the present work are presented in table 1 where it is seen that they agree well with both experimental measurements and with previous calculations in the literature.

In this case, the pure phonon eigenstate solutions to equation (5) at $\mathbf{q} = 0$ for $\nu = 4, 5, 6$ are degenerate, with $\omega^{\nu}(\mathbf{q} = 0) = 1069$ cm^{-1} and with Born coupling parameters $\mathcal{R}^{\nu}_{\alpha} = \mathcal{L}^{\nu}_{\alpha} = 2.63$ for $\alpha = x, y$, or z. For each choice of wavevector $\hat{\mathbf{q}}$ which defines the longitudinal direction and choice of transverse directions $\hat{\mathbf{T}}_1$ and $\hat{\mathbf{T}}_2$, there are three phonon–photon modes with frequencies $\omega_L(\mathbf{q})$ (from equation (26)), and $\omega_{T\pm}(\mathbf{q})$ (from equation (32)). In order to represent the phonon–photon modes in a conventional phonon band diagram, we must choose the wavevector values near $\mathbf{q} = 0$ along the special directions of the Brillouin zone. Because of the high symmetry of this crystal, the values of the electronic dielectric function $\epsilon^{\infty}_{\alpha\alpha}$ and the Born coupling parameter $\mathcal{R}^{\nu}_{\alpha}$ are the same for all directions α, the dispersion curves of $\omega_L(\mathbf{q})$ and $\omega_{T\pm}(\mathbf{q})$ have the same shape in each of the plotting directions, although their meanings differ. For example, consider the plot for $\mathbf{\Gamma} \to \mathbf{X}$ direction in the phonon band diagram. In this case, the longitudinal direction is $\hat{\mathbf{q}} = \hat{\mathbf{x}}$ while the transverse directions can be $\hat{\mathbf{T}}_1 = \hat{\mathbf{y}}$ and $\hat{\mathbf{T}}_2 = \hat{\mathbf{z}}$ or an equivalent permutation. As another example, consider the plot for $\mathbf{\Gamma} \to \mathbf{L}$ ($\langle 1\,1\,1 \rangle$ direction) in the phonon band diagram. In this case, the longitudinal direction is along the $\langle 1\,1\,1 \rangle$ direction, while the transverse directions are any two directions perpendicular to $\langle 1\,1\,1 \rangle$. Similarly, plotting the dispersions in the $\mathbf{\Gamma} \to \mathbf{K}$ ($\langle 1\,1\,0 \rangle$ direction) in the phonon band diagram means that the longitudinal mode is along the $\langle 1\,1\,0 \rangle$ direction while the transverse directions are perpendicular to $\langle 1\,1\,0 \rangle$. The phonon–photon dispersion curves are plotted in figure 4 in the $\mathbf{\Gamma} \to \mathbf{X}$ and $\mathbf{\Gamma} \to \mathbf{L}$ directions together with the pure phonon modes in a small range (1.4×10^4 cm^{-1}) of the Brillouin zone near $\mathbf{q} = 0$.

3.2.2. BN in a hexagonal structure. Figure 5 represents ball and stick diagrams of primitive cells of h-BN having the $P6_3/mmc$ structure and 4 atoms per primitive unit cell. The corresponding 12 phonon dispersion curves $\omega^{\nu}(\mathbf{q})$ as calculated by ABINIT were presented in figure 2. This structure of BN has less symmetry than that of the cubic phase but the dielectric tensors and Born effective charge tensors are diagonal having the form $Q_{xx} = Q_{yy}$ for tensor components representing the hexagonal layers and distinct values Q_{zz} representing components along the c-axis. Values of the dielectric tensor components, Born effective charge tensor components, and values of $\omega_{\text{TO}}(\mathbf{q} \gg \omega^{\nu} c/\sqrt{\epsilon^{\infty}_{T_i T_i}})$ and $\omega_{\text{LO}}(\mathbf{q} = 0)$ are listed in table 2 where they are compared with experiments and computations. In general, the present calculations are in good agreement with the literature except for the experimental values of ϵ_{zz} reported by Geick *et al* [21].

For hexagonal BN, it turns out that of the 12 normal modes at $\mathbf{q} = 0$, only three have nontrivial values of $\mathcal{R}^{\nu}_{\alpha} = \mathcal{L}^{\nu}_{\alpha}$. The lowest frequency mode that has a nontrivial value of $\mathcal{R}^{\nu}_{\alpha}$ is mode #7 with calculated frequency $\omega^{\nu}(\mathbf{q} = 0) = 752$ cm^{-1} and $\alpha = z$. The relative atomic displacements for this mode are illustrated in figure 5(a). In this case the non-zero Born coupling parameter is found to have the magnitude $\mathcal{R}^{\nu}_{z} = \mathcal{L}^{\nu}_{z} = 1.61$. The longitudinal mode is therefore along the $\hat{\mathbf{z}}$ axis, $\hat{\mathbf{q}} = \hat{\mathbf{z}}$, and the longitudinal frequency calculated from equation (26) is $\omega_L = 820$ cm^{-1} which can be plotted as a horizontal line on the phonon band diagram in the $\mathbf{\Gamma} \to \mathbf{A}$ direction. The corresponding transverse modes associated with this vibration can have the electric field along the $\hat{\mathbf{T}}_1 = \hat{\mathbf{z}}$ direction so that $\hat{\mathbf{q}}$ and $\hat{\mathbf{T}}_2$ are oriented along $\hat{\mathbf{x}}$ and $\hat{\mathbf{y}}$. In the conventional phonon band diagram, the two dispersive transverse modes $\omega_{T\pm}(\mathbf{q})$ could then be plotted along the $\mathbf{\Gamma} \to \mathbf{M}$ and $\mathbf{\Gamma} \to \mathbf{K}$ directions.

The other two normal modes with nontrivial values of $\mathcal{R}^{\nu}_{\alpha} = \mathcal{L}^{\nu}_{\alpha}$ are the doubly degenerate modes #11 and #12 with $\alpha = x$ and $\alpha = y$. The relative atomic displacements for one of these modes are indicated in figure 5(b). In this case, $\omega^{\nu}(\mathbf{q} = 0) = 1383$ cm^{-1} and the non-zero Born coupling parameter is found to have the magnitude $\mathcal{R}^{\nu}_{\alpha} = \mathcal{L}^{\nu}_{\alpha} = 5.35$ where $\alpha = x$ or $\alpha = y$. The nondispersive longitudinal frequency of this LO mode is calculated (via equation (26)) to be $\omega_L = 1614$ cm^{-1} and can be plotted along the $\mathbf{\Gamma} \to \mathbf{M}$ and $\mathbf{\Gamma} \to \mathbf{K}$ directions. For the case that $\alpha = x$, the corresponding transverse modes associated with this vibration have the electric field direction along the $\hat{\mathbf{T}}_1 = \hat{\mathbf{x}}$ direction so that $\hat{\mathbf{q}}$ and $\hat{\mathbf{T}}_2$ are oriented along $\hat{\mathbf{y}}$ and $\hat{\mathbf{z}}$. For the case that $\alpha = y$, the corresponding transverse modes associated with this vibration have the electric field direction along the $\hat{\mathbf{T}}_1 = \hat{\mathbf{y}}$ direction so that $\hat{\mathbf{q}}$ and $\hat{\mathbf{T}}_2$ are oriented along $\hat{\mathbf{z}}$ and $\hat{\mathbf{x}}$. Therefore, in the conventional phonon band diagram, the two dispersive transverse modes $\omega_{T_i\pm}(\mathbf{q})$ are then plotted along the $\mathbf{\Gamma} \to \mathbf{A}$ ($\hat{\mathbf{x}}$ or $\hat{\mathbf{y}}$ transverse to $\hat{\mathbf{z}}$) and $\mathbf{\Gamma} \to \mathbf{K}$ ($\hat{\mathbf{x}}$ transverse to $\hat{\mathbf{y}}$) or $\mathbf{\Gamma} \to \mathbf{M}$ ($\hat{\mathbf{y}}$ transverse to $\hat{\mathbf{x}}$), accordingly. For all three of the coupled phonon–photon modes, the analytical formulas of equations (26) and (32) apply. The results are plotted in figure 6 in a small range of $\mathbf{q}$ points near the $\mathbf{\Gamma}$ point of the Brillouin zone (3.9×10^4 cm^{-1}).

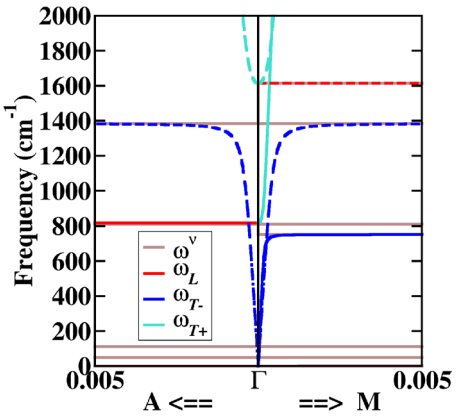

Figure 6. Phonon and phonon–photon dispersion curves in the vicinity of the **Γ** point of the Brillouin zone for h-BN. The plot includes **q** points in the direction $\mathbf{\Gamma} \rightarrow \mathbf{A}$ and in the direction $\mathbf{\Gamma} \rightarrow \mathbf{M}$ with the 0.005 tick marks indicating the value of **q** in units of the length of the $\mathbf{\Gamma} \rightarrow \mathbf{A}$ distance. The end points of the graph correspond to $|\mathbf{q}| = 3.9 \times 10^4$ cm^{-1}. The curves for ω^{ν} represent the modes calculated by ABINIT from equation (5) corrected for the TO-LO splitting as shown in figure 2. The coupled longitudinal modes are plotted in red while the coupled transverse modes are plotted in blue or turquoise as indicated. Dashed lines are used to distinguish curves associated with modes #11 and #12 from those associated with mode #7 drawn with full lines.

4. Summary and conclusions

In this report we set out to investigate the detailed origin of apparent discontinuities and mode disappearances in phonon band diagrams of ionic materials having hexagonal and other anisotropic structures. This resulted in a synthesis of the work of Huang [2, 3], Giannozzi *et al* [10], Gonze *et al* [12], Baroni *et al* [13], and others to derive the coupled equations for the ion motion and long wavelength electric fields using results from density functional theory and density functional perturbation theory. Current codes such as ABINIT and QUANTUM ESPRESSO include the effects on the longitudinal optical modes by introducing the so-called non-analytic correction to the second derivative matrix (equation (28)). In this work, we extend the analysis to include the transverse phonon–photon modes as well. The combination of the longitudinal and transverse phonon–photon mode dispersions are continuous functions of the wavevector **q** as has been demonstrated for cubic and hexagonal BN in figures 4 and 6, respectively. In principle, it should be possible to experimentally explore the transverse mode dispersions near $\mathbf{q} \rightarrow 0$. For example, Henry and Hopfield [47] showed that Raman spectroscopy can be used in a small angle scattering geometry to couple to the polariton. In a more recent example, heterostructures including hexagonal BN have been developed and measured with infrared microscopy to map the phonon–photon dispersion modes [48].

As a practical consideration, it may useful to further explore the use of the $\mathbf{q} = 0$ pure phonon mode basis (equation (16)) in order to analyze the longitudinal and transverse eigenvalues and eigenvectors as in equations (29), (30) and (36), (37).

Acknowledgments

This work was supported by NSF Grant DMR-1507942. Computations were performed on the Wake Forest University DEAC cluster, a centrally managed resource with support provided in part by the University. We would like to thank Fabien Bruneval and Josef Zwanziger for help with ABINIT commands.

Appendix. Some practical details

In practice, the phonon dispersion curves are usually evaluated not directly in units of angular frequency ω (rad/sec) but in units of wave number $\tilde{\omega} \equiv \omega/(2\pi c)$ (cm^{-1}), where c denotes the speed of light in vacuum. Therefore in order to evaluate the constants in equation (26) for example:

$$\frac{4\pi e^2}{\Omega M^{\nu}} \rightarrow \frac{1}{(2\pi c)^2}\frac{4\pi e^2}{\Omega M^{\nu}} \equiv 16\pi \left(\frac{e_H}{hc}\right)^2 \frac{1}{\Omega/a_B^3}\frac{1}{M^{\nu}/m_e}. \quad \text{(A.1)}$$

Here e_H denotes the ground state energy of a H atom, h denotes Planck's constant, a_B denotes the Bohr radius, and m_e denotes the electron mass.

ORCID iDs

Yan Li https://orcid.org/0000-0001-8253-7802
W C Kerr https://orcid.org/0000-0002-1281-8761
N A W Holzwarth https://orcid.org/0000-0001-5492-0660

References

[1] Li Y, Hood Z D and Holzwarth N A W 2019 Manuscript in preparation
[2] Huang K 1951 *Proc. R. Soc.* A **A208** 352–65
[3] Born M and Huang K 1954 *Dynamical Theory of Crystal Lattices* (Oxford: Oxford University Press)
[4] Kittel C 1963 *Quantum Theory of Solids* (New York: Wiley)
[5] Maradudin A A, Montroll E W, Weiss G H and Ipatova I P 1971 *Theory of Lattice Dynamics in the Harmonic Approximation* (*Solid State Physics: Supplement* vol 3) 2nd edn (New York: Academic)
[6] Böttger H 1983 *Principles of the Theory of Lattice Dynamics* (Weinheim: Physik Verlag)
[7] Setyawan W and Curtarolo S 2010 *Comput. Mater. Sci.* **49** 299–312
[8] Hohenberg P and Kohn W 1964 *Phys. Rev.* **136** B864–71
[9] Kohn W and Sham L J 1965 *Phys. Rev.* **140** A1133–8
[10] Giannozzi P, De Gironcoli S, Pavone P and Baroni S 1991 *Phys. Rev.* B **43** 7231
[11] Gonze X 1997 *Phys. Rev.* B **55** 10337–54
[12] Gonze X and Lee C 1997 *Phys. Rev.* B **55** 10355–68
[13] Baroni S, De Gironcoli S, Dal Corso A and Giannozzi P 2001 *Rev. Mod. Phys.* **73** 515
[14] Giannozzi P and Baroni S 2005 Density-functional perturbation theory *Handbook of Materials Modeling* ed S Yip (Berlin: Springer) p 195–214
[15] Gonze X *et al* 2016 *Comput. Phys. Commun.* **205** 106–31

[16] Giannozzi P *et al* 2017 *J. Phys.: Condens. Matter* **29** 465901
[17] Ghosez P and Gonze X 2000 *J. Phys.: Condens. Matter* **12** 9179–88
[18] Pick R M, Cohen M H and Martin R M 1970 *Phys. Rev.* B **1** 910–20
[19] Ghosez P, Michenaud J P and Gonze X 1998 *Phys. Rev.* B **58** 6224
[20] Irmer G, Röder C, Himcinschi C and Kortus J 2013 *Phys. Rev.* B **88** 104303
[21] Geick R, Perry C H and Rupprecht G 1966 *Phys. Rev.* **146** 543–7
[22] Gielisse P J, Mitra S S, Plendl J N, Griffis R D, Mansur L C, Marshall R and Pascoe E A 1967 *Phys. Rev.* **155** 1039–46
[23] Hoffman D M, Doll G L and Eklund P C 1984 *Phys. Rev.* B **30** 6051–6
[24] Jäger S, Bewilogua K and Klages C P 1994 *Thin Solid Films* **245** 50–4
[25] Eremets M I, Gauthier M, Polian A, Chervin J C, Besson J M, Dubitskii G A and Semenova Y Y 1995 *Phys. Rev.* B **52** 8854–63
[26] Reich S, Ferrari A C, Arenal R, Loiseau A, Bello I and Robertson J 2005 *Phys. Rev.* B **71** 205201
[27] Kutsay O *et al* 2010 *Diam. Relat. Mater.* **19** 968–71
[28] Cuscó R, Gil B, Cassabois G and Artús L 2016 *Phys. Rev.* B **94** 155435
[29] Karch K and Bechstedt F 1997 *Phys. Rev.* B **56** 7404–15
[30] Kern G, Kresse G and Hafner J 1999 *Phys. Rev.* B **59** 8551–9
[31] Ohba N, Miwa K, Nagasako N and Fukumoto A 2001 *Phys. Rev.* B **63** 115207
[32] Yu W J, Lau W M, Chan S P, Liu Z F and Zheng Q Q 2003 *Phys. Rev.* B **67** 014108
[33] Liu L, Feng Y P and Shen Z X 2003 *Phys. Rev.* B **68** 104102
[34] Cai Y, Zhang L, Zeng Q, Cheng L and Xu Y 2007 *Solid State Commun.* **141** 262–6
[35] Hamdi I and Meskini N 2010 *Physica* B **405** 2785–94
[36] Michel K H and Verberck B 2011 *Phys. Rev. B* **83** 115328
[37] Ontaneda J, Singh A, Waghmare U V and Grau-Crespo R 2018 *J. Phys.: Condens. Matter* **30** 185701
[38] Gruber T and Grüneis A 2018 *Phys. Rev.* B **98** 134108
[39] Blöchl P E 1994 *Phys. Rev.* B **50** 17953–79
[40] Holzwarth N A W, Tackett A R and Matthews G E 2001 *Comput. Phys. Commun.* **135** 329–47
[41] Perdew J P and Wang Y 1992 *Phys. Rev.* B **45** 13244–9
[42] Kokalj A 2003 *Comput. Mater. Sci.* **28** 155–68
[43] Momma K and Izumi F 2011 *Appl. Crystallogr.* **44** 1272–6
[44] Hahn T (ed) 2002 *International Tables for Crystallography, Volume A: Space-Group Symmetry, Fifth Revised Edition* (Boston, MA: Kluwer Academic)
[45] Eichhorn K, Kirfel A, Grochowski J and Serda P 1991 *Acta Crystallogr.* B **47** 843–8
[46] Pease R S 1952 *Acta Crystallographica* **5** 356–61
[47] Henry C H and Hopfield J J 1965 *Phys. Rev. Lett.* **15** 964–6
[48] Yang X, Zhai F, Hu H, Hu D, Liu R, Zhang S, Sun M, Sun Z, Chen J and Dai Q 2016 *Adv. Mater.* **28** 2931–8